Experimental and theoretical investigation of three-dimensional nitrogen-doped aluminum clusters Al_8N^- and Al_8N

Lei-Ming Wang,[1] Wei Huang,[1] Lai-Sheng Wang,[1,a)] Boris B. Averkiev,[2] and Alexander I. Boldyrev[2,b)]
[1]*Department of Physics, Washington State University, 2710 University Drive, Richland, Washington 99354, USA and Chemical and Materials Sciences Division, Pacific Northwest National Laboratory, MS K8-88, P.O. Box 999, Richland, Washington 99352, USA*
[2]*Department of Chemistry and Biochemistry, Utah State University, 0300 Old Main Hill, Logan, Utah 84322-0300, USA*

(Received 23 November 2008; accepted 19 February 2009; published online 1 April 2009)

The structure and electronic properties of the Al_8N^- and Al_8N clusters were investigated by combined photoelectron spectroscopy and *ab initio* studies. Congested photoelectron spectra were observed and experimental evidence was obtained for the presence of multiple isomers for Al_8N^-. Global minimum searches revealed several structures for Al_8N^- with close energies. The calculated vertical detachment energies of the two lowest-lying isomers, which are of C_{2v} and C_s symmetry, respectively, were shown to agree well with the experimental data. Unlike the three-dimensional structures of Al_6N^- and Al_7N^-, in which the dopant N atom has a high coordination number of 6, the dopant N atom in the two low-lying isomers of Al_8N^- has a lower coordination number of 4 and 5, respectively. The competition between the Al–Al and Al–N interactions are shown to determine the global minimum structures of the doped aluminum clusters and results in the structural diversity for both Al_8N^- and Al_8N. © *2009 American Institute of Physics*. [DOI: 10.1063/1.3097761]

I. INTRODUCTION

Doped clusters are interesting because they can exhibit specific properties tailored with the dopant. Understanding the structures and chemical bonding of such clusters may lead to rational designs of structurally and electronically stable clusters for applications in cluster-assembled nanomaterials or catalysis. While aluminum nitride is an important semiconductor material, there have been relatively few experimental and theoretical studies on small aluminum nitride clusters.[1–16] Li and Wang reported a set of photoelectron spectra of Al_xN^- ($x=2-22$) clusters at 193 nm and compared them to those of pure Al_x^- clusters.[10] They found spectral similarity between Al_xN^- and Al_{x-1}^- clusters and suggested that there is a strong charge transfer to form formally N^{3-} centers in the nitrogen-doped aluminum clusters. In a series of recent studies,[12,13,16] we combined photoelectron spectroscopy (PES) with global minimum structural search, using a gradient-embedded genetic algorithm followed by high-level *ab initio* calculations, to elucidate the detailed atomic structures and chemical bonding for several small nitrogen-doped aluminum clusters, Al_xN^- ($x=3-7$). It was shown that Al_xN^- clusters are planar for $x=3-5$, whereas their global minimum structures became three-dimensional (3D) for $x=6$ and 7 with the nitrogen atom having a coordination number of six.

In the current work, we continue our research on Al_xN^- clusters and report the geometric and electronic structures of the Al_8N^- cluster using PES and *ab initio* calculations. Congested PES spectra were observed and interpreted by the *ab initio* data. A few different structures have been suggested theoretically for Al_8N and Al_8N^- in previous studies,[7–9] but they have not been confirmed experimentally. We found that there are several low-lying isomers for Al_8N^-, which are all 3D and very close in energy. Photoelectron spectra of Al_8N^- have been obtained at different experimental conditions, confirming the presence of close-lying isomers that contribute to the experiment. The coordination numbers of the nitrogen atom in these low-lying isomers of Al_8N^- vary from 4 to 6. Unlike the 3D clusters of Al_6N^- and Al_7N^-, the N-centered $[Al_6N]^{3-}$ octahedron is no longer found as a building block in the two lowest energy structures of Al_8N^-.

II. EXPERIMENTAL METHOD

The experiment was performed on a magnetic-bottle PES apparatus with a laser vaporization cluster source, details of which have been published elsewhere.[17] Briefly, the Al_8N^- clusters were produced by laser vaporization of an Al/AlN composite disk target using a pure helium carrier gas. The cluster/He gas mixture passed through a 10 cm long, 3 mm diameter tube extension to allow adequate thermalization of the clusters. This was found to produce relatively cold clusters, which were shown to be important to yield well-resolved PES spectra.[18,19] The anion clusters were extracted from the cluster beam perpendicularly and were analyzed using a time-of-flight mass spectrometer. Only Al_xN^- clusters with one N impurity atom could be observed under the experimental condition, as was shown before.[10] The Al_8N^- cluster was mass selected and decelerated before being photodetached by a 193 nm laser beam from an ArF

a)Electronic mail: ls.wang@pnl.gov.
b)Electronic mail: a.i.boldyrev@usu.edu.

excimer laser, or by a 355 or 266 nm beam from a neodymium-doped yttrium aluminum garnet laser. Photoelectrons were collected at near 100% collecting efficiency by the magnetic bottle and analyzed using a 3.5 m long electron flight tube. The electron energies were calibrated by the known spectrum of Au^- (193 nm) or Rh^- (355 and 266 nm). The resolution ($\Delta E_k/E_k$) of the apparatus was about 2.5%, i.e., ~25 meV for 1 eV kinetic energy electrons.

III. THEORETICAL METHODS

We performed initial computational search for the global minima of Al_8N^- and Al_8N using both our gradient embedded genetic algorithm (GEGA) program written by Alexandrova *et al.*[20,21] and our simulated annealing program written by Call and co-workers.[16] We used a hybrid method known as B3LYP[22–24] with the small split-valence basis set (3-21G) for energy, gradient, and force calculations, with simulated annealing performing single-point energy calculations and GEGA performing gradient optimizations and frequency calculations. We reoptimized geometries and calculated frequencies for the lowest isomers using the B3LYP and CCSD(T)[25–27] methods with the polarized split-valence basis set (6-311+G*).[28–30] Total energies of the lowest isomers were also calculated using the CCSD(T) method with the extended 6-311+G(2*df*) basis set at the optimized CCSD(T)/6-311+G* geometries.

The vertical electron detachment energies (VDEs) were calculated using the RCCSD(T)/6-311+G(2*df*) method, the restricted outer valence Green Function method (ROVGF/6-311+G(2*df*))[31–35] all at the optimized RCCSD(T)/6-311+G* geometries and the time-dependent DFT method[36,37] (TD-B3LYP/6-311+G(2*df*)) at the optimized B3LYP/6-311+G* geometries. In the last approach, the first VDE was calculated at the B3LYP level of theory as the lowest transition from the singlet state of the anion into the final lowest doublet state of the neutral. Then the vertical excitation energies of the neutral species (at the TD-B3LYP level) were added to the first VDE to obtain the second and higher VDEs. Core electrons were frozen in treating the electron correlation at the RCCSD(T) and ROVGF levels of theory. The B3LYP, RCCSD(T), ROVGF, and TD-B3LYP calculations were performed using the GAUSSIAN 03 and MOLPRO programs.[38,39] Molecular structure visualization was done using the MOLDEN 3.4 program.[40]

IV. EXPERIMENTAL RESULTS

Figure 1 shows the PES spectra of Al_8N^- at three different photon energies. At 355 nm [Fig. 1(a)], two relatively sharp bands (*X* and *A*) were observed at VDEs of 2.86 and 3.16 eV, respectively. The adiabatic detachment energy (ADE) was evaluated from the relatively sharp onset of the *X* band to be 2.75 ± 0.05 eV. A shoulder (*X'*) on the high binding energy side of band *X* was discernible, which became more obvious in the 266 nm spectrum [Fig. 1(b)]. In addition, the 266 nm spectrum revealed several new bands: *B*, *C*, *D*, *E*, and *F*. The *A* band seems to show some fine features on its high binding energy side around ~3.3 eV, which could be due to vibrational structures and/or additional electronic transitions. However, the pattern of the fine features seemed to depend on experimental conditions, indicating that they may be from different isomers. At 193 nm [Fig. 1(c)], a new band *G* was observed at ~4.6 eV, but featureless and continuous signals were observed beyond 4.8 eV. The overall PES spectral pattern was quite congested and complicated, probably due to contributions from more than one isomer. The VDEs of all observed bands are listed in Table I and compared with the theoretical data in Table II.

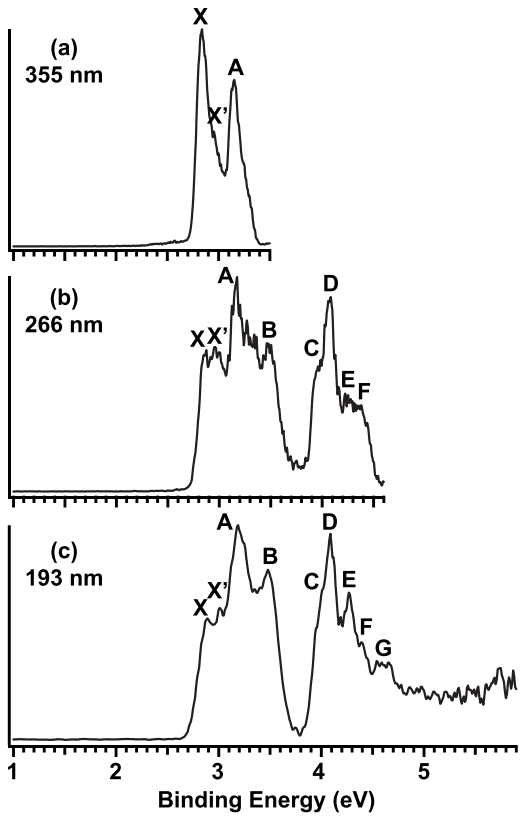

FIG. 1. Photoelectron spectra of Al_8N^- at (a) 355 nm (3.496 eV), (b) 266 nm (4.661 eV), and (c) 193 nm (6.424 eV).

To affirm the presence of low-lying isomers, we also measured PES spectra under "hot" conditions without using the tube extension in the cluster source, as shown in Fig. 2. These spectra all show a long tail at the low binding energy side due to hot band transitions, implying that clusters gen-

TABLE I. Experimentally observed VDE and ADE of Al_8N^- from its photoelectron spectra (the numbers in the parentheses represent the experimental uncertainties in the last digit).

Observed features	VDE (eV)	ADE (eV)
X	2.86(4)	2.75(5)
X'	2.99(5)	
A	3.16(3)	
B	3.45(5)	
C	~4.0	
D	4.09(3)	
E	4.26(5)	
F	4.40(5)	
G	~4.6	

TABLE II. The calculated VDEs of Al_8N^- for isomers I, II, and III at different levels of theory, and comparisons to the experimental data.

		VDE (Theo.) (eV)			PES assignments	
Isomer	Final states and configuration	TD-DFT	ROVGF[a]	RCCSD(T)	Features	VDE (exp.) (eV)[b]
I	$^2B_2, 5a_1^2 3b_2^2 6a_1^2 1a_2^2 3b_1^2 7a_1^2 4b_2^1$	2.64	2.79(0.87)	2.89	*X*	2.86(4)
	$^2A_1, 5a_1^2 3b_2^2 6a_1^2 1a_2^2 3b_1^2 7a_1^1 4b_2^2$	2.96	3.09(0.87)	3.25	*A*	3.16(3)
	$^2B_1, 5a_1^2 3b_2^2 6a_1^2 1a_2^2 3b_1^1 7a_1^2 4b_2^2$	3.28	3.09(0.86)	3.33	*A* tail	~3.3
	$^2A_2, 5a_1^2 3b_2^2 6a_1^2 1a_2^1 3b_1^2 7a_1^2 4b_2^2$	3.17	3.34(0.86)	3.42	*B*	3.45(5)
	$^2A_1, 5a_1^2 3b_2^2 6a_1^1 1a_2^2 3b_1^2 7a_1^2 4b_2^2$	3.86	3.92(0.86)		*C*	~4.0
	$^2B_2, 5a_1^2 3b_2^1 6a_1^2 1a_2^2 3b_1^2 7a_1^2 4b_2^2$	3.89	4.23(0.86)		*E*	4.26(5)
	$^2A_1, 5a_1^1 3b_2^2 6a_1^2 1a_2^2 3b_1 7a_1^2 4b_2^2$	4.32	4.38(0.85)		*F*	4.40(5)
II	$^2A', 6a'^2 7a'^2 3a''^2 8a'^2 4a''^2 9a'^2 5a''^2 10a'^1$	2.73	2.77(0.87)	2.93	*X'*	2.99(5)
	$^2A'', 6a'^2 7a'^2 3a''^2 8a'^2 4a''^2 9a'^2 5a''^1 10a'^2$	2.95	3.16(0.86)	3.28	*A*	3.16(3)
	$^2A', 6a'^2 7a'^2 3a''^2 8a'^2 4a''^2 9a'^1 5a''^2 10a'^2$	3.24	3.30(0.86)		*A* tail	~3.3
	$^2A'', 6a'^2 7a'^2 3a''^2 8a'^2 4a''^1 9a'^2 5a''^2 10a'^2$	3.18	3.35(0.86)		*A* tail	~3.3
	$^2A', 6a'^2 7a'^2 3a''^2 8a'^1 4a''^2 9a'^2 5a''^2 10a'^2$	4.04	4.11(0.84)		*D*	4.09(3)
	$^2A'', 6a'^2 7a'^2 3a''^1 8a'^2 4a''^2 9a'^2 5a''^2 10a'^2$	4.15	4.38(0.83)		*F*	4.40(5)
	$^2A', 6a'^2 7a'^1 3a''^2 8a'^2 4a''^2 9a'^2 5a''^2 10a'^2$	4.52	4.88(0.81)		*G*	~4.6
	$^2A', 6a'^1 7a'^2 3a''^2 8a'^2 4a''^2 9a'^2 5a''^2 10a'^2$	5.24	5.18(0.77)			
III	$^2B_2, 2b_1^2 5a_1^2 1a_2^2 6a_1^2 3b_2^2 3b_1^2 7a_1^2 4b_2^1$	2.83	3.17(0.87)	3.12	*A*	3.16(3)
	$^2A_1, 2b_1^2 5a_1^2 1a_2^2 6a_1^2 3b_2^2 3b_1^2 7a_1^1 4b_2^2$	2.98	3.22(0.86)	3.24	*A* tail	~3.3
	$^2B_1, 2b_1^2 5a_1^2 1a_2^2 6a_1^2 3b_2^2 3b_1^1 7a_1^2 4b_2^2$	3.25	3.47(0.85)	3.49	*B*	3.45(5)
	$^2B_2, 2b_1^2 5a_1^2 1a_2^2 6a_1^2 3b_2^1 3b_1^2 7a_1^2 4b_2^2$	3.92	3.96(0.85)		*C*	~4.0
	$^2A_1, 2b_1^2 5a_1^2 1a_2^2 6a_1^1 3b_2^2 3b_1^2 7a_1^2 4b_2^2$	4.12	4.32(0.84)		*E*	4.26(5)
	$^2A_2, 2b_1^2 5a_1^2 1a_2^1 6a_1^2 3b_2^2 3b_1^2 7a_1^2 4b_2^2$	4.74	4.92(0.84)	4.92		
	$^2A_1, 2b_1^2 5a_1^1 1a_2^2 6a_1^2 3b_2^2 3b_1^2 7a_1^2 4b_2^2$	4.79	4.98(0.84)			
	$^2B_1, 2b_1^1 5a_1^2 1a_2^2 6a_1^2 3b_2^2 3b_1^2 7a_1^2 4b_2^2$	4.64	4.94(0.82)			

[a]Numbers in the parentheses represent the pole strength of the OVGF calculation.
[b]Numbers in the parentheses represent the experimental uncertainties in the last digit.

erated under this condition were indeed relatively hot. A major difference observed between these two sets of data is that the relative intensity of the *X'* band seems to be enhanced in the "hot" spectra. Note that this is most clearly displayed in the 355 nm spectra. In the 193 nm spectra, all the detachment bands are heavily overlapped due to reduced resolution, so the slight variation in relative intensities is more difficult to distinguish. Even at 266 nm, the spectral congestion made it difficult to compare relative intensity variations at the two experimental conditions. Nevertheless, our data provide clear experimental evidence that at least the *X'* band should come from contributions by another isomer. The overall congested spectra are consistent with the presence of multiple isomers, because we observed less congested spectra even for larger Al_nN^- clusters.[10] As will be shown below, this is indeed borne by our theoretical calculations.

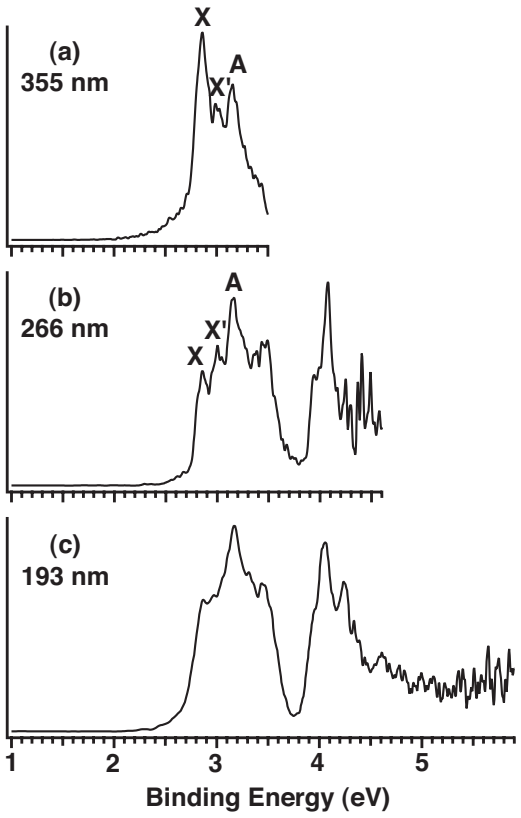

FIG. 2. Same as Fig. 1, but taken under hotter source conditions.

V. THEORETICAL RESULTS

A. Al_8N^-

We initially performed simulated annealing and GEGA searches for the global minimum of Al_8N^- at the B3LYP/3-21G level of theory separately for singlet and triplet states. Both methods revealed an identical global minimum structure II (C_s, $^1A'$) (Fig. 3). The geometries and frequencies for the low-lying structures of Al_8N^- were then recalculated at the B3LYP/6-311+G* level of theory. Finally, single point

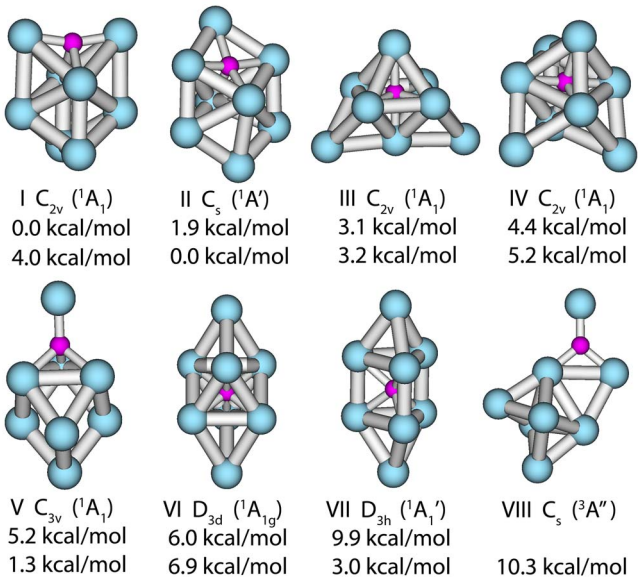

FIG. 3. (Color online) The first seven low-lying singlet isomers and the lowest triplet isomer of Al_8N^-. Upper and lower numbers are relative energies calculated at the CCSD(T)/6-311+G(2*df*)//CCSD(T)/6-311+G* +ZPE//B3LYP/6-311+G* and B3LYP/6-311+G*+ZPE//B3LYP/6-311 +G* levels of theory, respectively.

calculations for the seven lowest-lying isomers were calculated at RCCSD(T)/6-311+G(2*df*) at the optimized CCSD(T)/6-311+G* structures. Geometries, symmetry, electronic state, and relative energies at B3LYP/6-311+G* and at CCSD(T)/6-311+G(2*df*)//CCSD(T)/6-311+G* +ZPE//B3LYP/6-311+G* for the first seven low-lying singlet and the lowest triplet isomers of Al_8N^- are displayed in Fig. 3.

The structure II ($^1A'$, $1a'^2 2a'^2 1a''^2 3a'^2 4a'^2 2a''^2 5a'^2 6a'^2 7a'^2 3a''^2 8a'^2 4a''^2 9a'^2 5a''^2 10a'^2$) (the molecular orbitals are arranged according to its VDEs) of C_s symmetry was found to be the global minimum (Fig. 3) at both the B3LYP/3-21G and the B3LYP/6-311+G* levels of theory. However, at the CCSD(T)/6-311+G(2*df*)//CCSD(T)/6-311+G* +ZPE//B3LYP/6-311+G* level of theory the structure I ($^1A_1$, $1a_1^2 2a_1^2 1b_2^2 1b_1^2 3a_1^2 2b_2^2 2b_1^2 4a_1^2 5a_1^2 3b_2^2 6a_1^2 1a_2^2 3b_1^2 7a_1^2 4b_2^2$) of C_{2v} symmetry is lower than structure II by 1.9 kcal/mol. It should be stressed that from the theoretical point of view, such a small energy difference is beyond our ability to determine the global minimum structure of this anion with certainty. Unlike the 3D global minimum structures of Al_6N^- and Al_7N^-, in which the nitrogen atom has a high coordination number of 6,[13,16] in both low-lying isomers of Al_8N^- (I and II), the nitrogen atom has low coordination numbers of 4 and 5, respectively. Structure I can be described as an Al_6 octahedron bonded by an Al–N–Al motif. On the basis of the natural population analysis the Al–N–Al motif carries formal negative charge of −1. Structure II can be considered as originating from structure I by moving one bottom aluminum atom from the Al_6 octahedron to the top to bond with the N atom. Both isomers I and II seem to have been missed in a previous study by Leskiw *et al.*[7]

The next five low-lying isomers of Al_8N^- were found to be 3.1 kcal/mol (isomer III), 4.4 kcal/mol (isomer IV), 5.2 kcal/mol (isomer V), 6.0 kcal/mol (isomer VI), and 9.9 kcal/mol (isomer VII) higher in energy than the global minimum (isomer I) at the CCSD(T)/6-311 +G(2*df*)//CCSD(T)/6-311+G*+ZPE//B3LYP/6-311+G* level of theory. Structures III–VII have the following symmetry, electronic state, and configuration,

III-C_{2v}, $^1A_1$, $1a_1^2 1b_2^2 2a_1^2 1b_1^2 3a_1^2 2b_2^2 4a_1^2 2b_1^2 5a_1^2 1a_2^2 6a_1^2 3b_2^2 3b_1^2 7a_1^2 4b_2^2$,

IV-C_{2v}, $^1A_1$, $1a_1^2 2a_1^2 1b_2^2 1b_1^2 3a_1^2 2b_2^2 4a_1^2 2b_1^2 5a_1^2 3b_1^2 3b_2^2 6a_1^2 1a_2^2 7a_1^2 4b_2^2$,

V-C_{3v}, $^1A_1$, $1a_1^2 2a_1^2 3a_1^2 1e^4 2e^4 4a_1^2 5a_1^2 3e^4 6a_1^2 4e^4 7a_1^2$,

VI-D_{3d}, $^1A_{1g}$, $1a_{1g}^2 1a_{2u}^2 1e_u^4 2a_{1g}^2 2a_{2u}^2 3a_{1g}^2 2e_u^4 1e_g^4 3a_{2u}^2 2e_g^4 4a_{1g}^2$,

VII-D_{3h}, $^1A_1'$, $1a_1'^2 1a_2''^2 1e'^4 2a_1'^2 2a_2''^2 3a_1'^2 2e'^4 1e''^4 3a_2''^2 4a_1'^2 3e'^4$.

Isomers III, IV, and VI can be considered as all three possible combinations of the Al_6N^{3-} octahedron bicapped by two formal Al^+ cations. We discussed the structure and bonding of the perfect octahedral Al_6N^{3-} previously.[13] Structure V can be viewed as a distorted aluminum octahedron bicapped with an Al and an Al–N fragment to opposite sides. Finally, structure VII is formally a trigonal prism Al_6N^{3-} bicapped by two Al^+ cations.

B. Al_8N

We also performed simulated annealing and GEGA searches for the global minimum structure of neutral Al_8N at the B3LYP/3-21G level of theory for both doublet and quartet states. The geometries and frequencies for low-lying structures were then recalculated at B3LYP/6-311+G* level. Finally, single point calculations for the low-lying isomers were calculated at RCCSD(T)/6-311+G(2*df*) at the

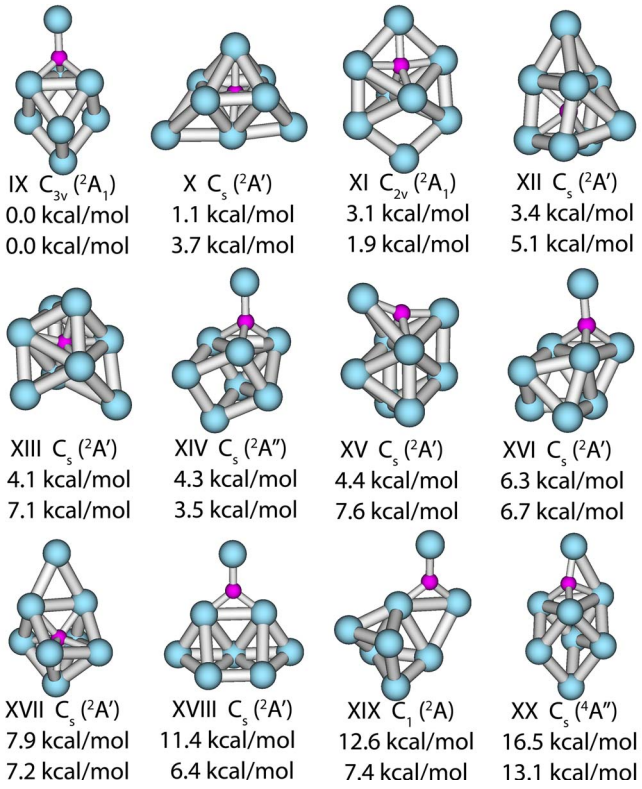

FIG. 4. (Color online) The first eleven low-lying doublet isomers and the lowest quartet isomer of Al_8N. Upper and lower numbers are relative energies calculated at the CCSD(T)/6-311+G(2*df*)//B3LYP/6-311+G* +ZPE//B3LYP/6-311+G* and B3LYP/6-311+G*+ZPE//B3LYP/6-311 +G* levels of theory, respectively.

optimized B3LYP/6-311+G* geometries. The structures of the eleven lowest-lying doublet isomers and one lowest quartet isomer of Al_8N are shown in Fig. 4.

According to our GEGA search, isomer IX was found to be the global minimum structure (Fig. 4). This structure (C_{3v}, $^2A_1$, $1a_1^2 2a_1^2 3a_1^2 1e^4 2e^4 4a_1^2 5a_1^2 3e^4 6a_1^2 4e^4 7a_1^1$) can be viewed as generated from structure V of the anion by removing one electron from its doubly occupied highest occupied molecular orbital (HOMO). The next lowest structure is structure X (C_s, $^2A'$, $1a'^2 2a'^2 1a''^2 3a'^2 4a'^2 5a'^2 6a'^2 7a'^2 2a''^2 3a''^2 8a'^2 9a'^2 4a''^2 10a'^2 11a'^1$), which is only 1.1 kcal/mol higher in energy at RCCSD(T)/6-311 +G*//B3LYP/6-311+G*+ZPE//B3LYP/6-311+G* level, and thus they are degenerate from our point of view. The isomers X, XI, XIII, XV, and XIX can be viewed as derived from the anionic isomers III, II, IV, I, and VIII, respectively, by removing one electron from the HOMO and some subsequent bond relaxation. It is more difficult to find parental anionic isomers for the neutral isomers XII, XIV, XVI, XVII, XVIII, and XX. We notice that similar structures as isomer X, XI, and XII have been reported previously for Al_8N by several groups.[7–9] Similar to the case of the anionic isomers, the potential energy surface of the neutral Al_8N cluster is found to have many low-lying local minima.

VI. INTERPRETATION OF THE PES SPECTRA

Our extensive structural search for Al_8N^- revealed five low-lying isomers within about less than 5 kcal/mol

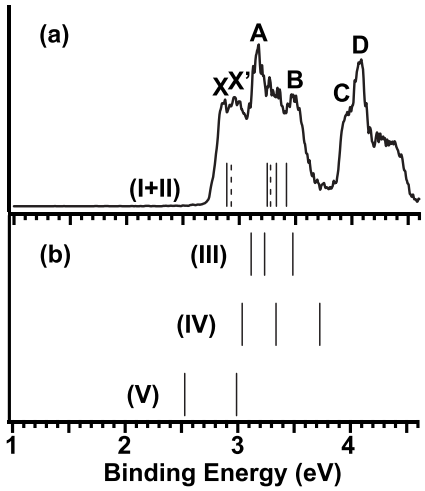

FIG. 5. Comparison of the 266 nm PES spectra with the calculated VDEs (shown as vertical bars) at the RCCSD(T)/6-311+G(2df) level for (a) isomer I (solid line bars) and isomer II (dashed line bars), (b) isomers III, IV, and V of Al_8N^-.

at the CCSD(T)/6-311+G(2*df*)//CCSD(T)/6-311+G* +ZPE//B3LYP/6-311+G* level of theory (Fig. 3). Those isomers are so close in energies that potentially they could all contribute to the experimentally observed PES spectra. Indeed, the congested spectral pattern of Al_8N^- suggested potential complications due to the presence of more than one isomer, as evidenced experimentally (Figs. 1 and 2). To aid the assignments, the calculated VDEs of the first few detachment channels for these five low-lying isomers of Al_8N^- at our highest level of theory, RCCSD(T)/6-311+G(2*df*), are compared to the 266 nm PES spectrum in Fig. 5, where the calculated VDEs are plotted as vertical bars. Clearly, isomer V ($^1A_1$, C_{3v}) can be ruled out, because its first VDE is very low at 2.53 eV [Fig. 5(b)], which is absent in the experimental data. Similarly, the third VDE of isomer IV ($^1A_1$, C_{3v}) occurs in the gap region of the PES spectra and it is expected to have negligible contributions to the observed spectrum. Both isomers IV and V are relatively high in energy and it is reasonable that they are not present in our experiment.

The first VDE of the lowest energy isomer I ($^1A_1$, C_{2v}) agrees well with the *X* band [Fig. 5(a)]. However, its second VDE calculated at RCCSD(T) is 3.25 eV, much larger than the experimental VDE (2.99 eV) of the second band (X'), indicating that the observed PES spectra cannot be explained by a single isomer I. As discussed above, the experimental observation suggests the X' band to be contributed by another isomer. Indeed, the first VDE (2.93 eV) of isomer II ($^1A'$, C_s), which is only 1.9 kcal/mol at the CCSD(T) level above isomer I, matches the X' band (2.99 eV) quite well [Fig. 5(a)]. Thus, isomers I and II should be the major carriers of the PES spectra. As seen in Fig. 5(b), isomer III ($^1A_1$, C_{2v}) also gives detachment transition features, which are within the observed PES pattern. While we cannot assign this isomer definitively, we also cannot completely rule it out. According to our calculations, isomer III is 3.1 kcal/mol above the global minimum, so its population, if there is any, should be much smaller relative to isomers I and II and can be ruled out in our assignments. The calculated VDEs for

isomers I, II, and III of Al_8N^- at the TD-B3LYP/6-311+G(2*df*), ROVGF/6-311+G(2*df*), and RCCSD(T)/6-311+G(2*df*) levels of theory are presented in Table II, as well as the tentative spectral assignments. We can see that higher energy detachment channels of these isomers are also consistent with the PES data.

Overall, the experimental data are in good agreement with the combined detachment transitions calculated for the two lowest isomers (I and II), indicating that these structures are competing for the global minimum of Al_8N^-. The higher energy of isomer II is consistent with its slightly enhanced population under hotter experimental conditions, indicating that isomer I should be the true global minimum for Al_8N^- and confirming the accuracy of the current level of theory.

VII. DISCUSSION

One of the most striking results found in the current experimental and theoretical study of Al_8N^- and Al_8N is the presence of structurally diverse isomers with close energies. This is likely a result of increasing competition between Al–Al and Al–N interactions in the doped cluster. In the smaller doped clusters, Al_xN^- and Al_xN ($x=3-5$),[12] the Al–N interactions are more important. For example, in the Al_3N^- (C_{2v}) and Al_4N^- (D_{4h}) clusters, all aluminum atoms are located in the first coordination layer of the central nitrogen atom in planar geometries, which optimize the Al–N interactions.[12] We started to encounter low-lying isomers in Al_5N^- due to the competition between Al–Al and Al–N interactions. The global minimum structure of Al_5N^- (C_{2v}) is built upon the square-planar Al_4N^- structure with the additional Al atom boned to one of its four edges outside the first coordination layer. However, a 3D structure, which can be viewed as a tetrahedral Al_4 cluster bound to an AlN unit, was found to be a low-lying isomer and was also present in the PES spectra of Al_5N^-.[12] Thus, the Al–Al interactions start to be important structure-forming factors in Al_5N^-. For Al_6N^-, we found two close low-lying isomers, which appear to optimize both the Al–Al and Al–N interactions.[13] For Al_7N^- and Al_7N, our study found only one dominating isomer in which the N atom has high coordination number of 6 and 7, respectively. Particularly for Al_7N, the seven Al atoms are all in the first coordination sphere and bound to the N atom, which seems to optimize Al–N interactions.[16] We have also shown that the global minimum structures of the Al_6N^- and Al_7N^- can be viewed as being evolved from the N-centered Al_6N^{3-} octahedron. The chemical bonding in the Al_6N^{3-} octahedron can be approximately rationalized as the central N atom carrying an effective charge of -3 (N^{3-}), which is ionically bound to an octahedral Al_6 cluster, thus optimizing both Al–Al and Al–N interactions.

For Al_8N^-, this Al_6N^{3-} octahedron is no longer found as a building block in the two lowest-lying isomers (Fig. 3). Instead, the two lowest isomers (I and II) of Al_8N^- can both be viewed as a distorted Al_4N^- square bound to four additional Al atoms. Unlike the 3D structures of Al_6N^- and Al_7N^-, the Al–Al interactions seem to be dominating in Al_8N^-, although isomers III and IV do contain the Al_6N^{3-} octahedron units and they are not too high in energy. Thus, the more complicated balance between Al–Al and Al–N interactions in the larger Al_8N^- cluster are responsible for its structural diversity. It should also be pointed out that in all the low-lying isomers for Al_8N^- we found that the effective atomic charges on the N atom (calculated using natural bond analysis at B3LYP/6-311+G*) vary from $-2.1|e|$ to $-2.5|e|$, indicating the formation of the nearly complete shell $2s^22p^6$ in the ionic limit (N^{3-}), which is consistent with the previous experimental observations.[10]

VIII. SUMMARY

We investigated the structural properties of the Al_8N^- cluster using a combined PES and *ab initio* study. The calculated VDEs were compared to the complicated PES spectral features and confirmed the presence of multiple isomers in the experiment for Al_8N^-. The global minimum structures of Al_8N and Al_8N^- were located using both genetic algorithm and simulated annealing. We found that at least two low-lying isomers of Al_8N^- were populated experimentally and contribute to the observed PES spectra. Unlike the 3D structures of Al_6N^- and Al_7N^-, where the N atom has a high coordination number of 6, in the two low-lying isomers of Al_8N^-, the N atom has low coordination numbers of 4 and 5. The competition between Al–Al and Al–N interactions are found to dictate the structures of the N-doped aluminum clusters and results in the diverse low-lying structures for Al_8N^- and Al_8N.

ACKNOWLEDGMENTS

The theoretical work done at Utah State University was supported by the National Science Foundation (Grant No. CHE-0714851). Computer time from the Center for High Performance Computing at Utah State University is gratefully acknowledged. The computational resource, the Uinta cluster supercomputer, was provided through the National Science Foundation under Grant No. CTS-0321170 with matching funds provided by Utah State University. The experimental work done at Washington State University was supported by the National Science Foundation (Grant No. DMR-0503383) and was performed at the W. R. Wiley Environmental Molecular Sciences Laboratory, a national scientific user facility sponsored by the DOE Office of Biological and Environmental Research and located at Pacific Northwest National Laboratory, which is operated for DOE by Battelle.

[1] P. v. R. Schleyer and A. I. Boldyrev, J. Chem. Soc., Chem. Commun. 1536 (1991).
[2] V. G. Zakrzewski, W. v. Niessen, A. I. Boldyrev, and P. v. R. Schleyer, Chem. Phys. **174**, 167 (1993).
[3] S. K. Nayak, S. N. Khana, and P. Jena, Phys. Rev. B **57**, 3787 (1998).
[4] S. K. Nayak, B. K. Rao, P. Jena, X. Li, and L. S. Wang, Chem. Phys. Lett. **301**, 379 (1999).
[5] B. H. Boo and Z. Liu, J. Phys. Chem. A **103**, 1250 (1999).
[6] L. Andrews, M. Zhou, G. V. Chertihin, W. D. Bare, and Y. Hannachi, J. Phys. A **104**, 1656 (2000).
[7] B. R. Leskiw, A. W. Castleman, Jr., C. Ashman, and S. N. Khanna, J. Chem. Phys. **114**, 1165 (2001).
[8] L. Ling, B. Song, and P.-L. Cao, J. Mol. Struct.: THEOCHEM **728**, 215 (2005).

[9] L. Guo and H.-S. Wu, Int. J. Quantum Chem. **106**, 1250 (2006).
[10] X. Li and L. S. Wang, Eur. Phys. J. D **34**, 9 (2005).
[11] G. Meloni, S. M. Sheehan, B. F. Parsons, and D. M. Neumark, J. Phys. Chem. A **110**, 3527 (2006).
[12] B. B. Averkiev, A. I. Boldyrev, X. Li, and L. S. Wang, J. Chem. Phys. **125**, 124305 (2006).
[13] B. B. Averkiev, A. I. Boldyrev, X. Li, and L. S. Wang, J. Phys. Chem. A **111**, 34 (2007).
[14] B. Wang, D. Shi, X. Chen, G. Wang, and J. Zhao, Int. J. Mod. Phys. B **19**, 2380 (2005).
[15] Q. Sun, Q. Wang, X. G. Gong, V. Kumar, and Y. Kawazoe, Eur. Phys. J. D **18**, 77 (2002).
[16] B. B. Averkiev, S. Call, A. I. Boldyrev, L. M. Wang, W. Huang, and L. S. Wang, J. Phys. Chem. A **112**, 1873 (2008).
[17] L. S. Wang, H. S. Cheng, and J. Fan, J. Chem. Phys. **102**, 9480 (1995).
[18] X. Li, H. Wu, X. B. Wang, and L. S. Wang, Phys. Rev. Lett. **81**, 1909 (1998).
[19] J. Akola, M. Manninen, H. Hakkinen, U. Landman, X. Li, and L. S. Wang, Phys. Rev. B **60**, R11297 (1999).
[20] A. N. Alexandrova, A. I. Boldyrev, Y.-J. Fu, X. B. Wang, and L. S. Wang, J. Chem. Phys. **121**, 5709 (2004).
[21] A. N. Alexandrova and A. I. Boldyrev, J. Chem. Theory Comput. **1**, 566 (2005).
[22] A. D. Becke, J. Chem. Phys. **98**, 5648 (1993).
[23] S. H. Vosko, L. Wilk, and M. Nusair, Can. J. Phys. **58**, 1200 (1980).
[24] C. Lee, W. Yang, and R. G. Parr, Phys. Rev. B **37**, 785 (1988).
[25] J. Čížek, Adv. Chem. Phys. **14**, 35 (1969).
[26] P. J. Knowles, C. Hampel, and H.-J. Werner, J. Chem. Phys. **99**, 5219 (1993).
[27] K. Raghavachari, G. W. Trucks, J. A. Pople, and M. Head-Gordon, Chem. Phys. Lett. **157**, 479 (1989).
[28] J. S. Binkley, J. A. Pople, and W. J. Hehre, J. Am. Chem. Soc. **102**, 939 (1980); M. S. Gordon, J. S. Binkley, J. A. Pople, W. J. Pietro, and W. J. Hehre, *ibid.* **104**, 2797 (1982); W. J. Pietro, M. M. Francl, W. J. Hehre, D. J. Defrees, J. A. Pople, and J. S. Binkley, *ibid.* **104**, 5039 (1982).
[29] A. D. McLean and G. S. Chandler, J. Chem. Phys. **72**, 5639 (1980).
[30] T. Clark, J. Chandrasekhar, G. W. Spitznagel, and P. v. R. Schleyer, J. Comput. Chem. **4**, 294 (1983).
[31] L. S. Cederbaum, J. Phys. B **8**, 290 (1975).
[32] J. V. Ortiz, Int. J. Quantum Chem., Quantum Chem. Symp. **23**, 321 (1989); J. S. Lin and J. V. Ortiz, Chem. Phys. Lett. **171**, 197 (1990).
[33] V. G. Zakrzewski, J. V. Ortiz, J. A. Nichols, D. Heryadi, D. L. Yeager, and J. T. Golab, Int. J. Quantum Chem. **60**, 29 (1996).
[34] Y. Dahnovsky, J. Chem. Phys. **126**, 234111 (2007).
[35] A. Kletsov and Y. Dahnovsky, Phys. Rev. B **76**, 035304 (2007).
[36] R. Bauernschmitt and R. Alrichs, Chem. Phys. Lett. **256**, 454 (1996).
[37] M. E. Casida, C. Jamorski, K. C. Casida, and D. R. Salahub, J. Chem. Phys. **108**, 4439 (1998).
[38] M. J. Frisch, G. W. Trucks, H. B. Schlegel *et al.*, GAUSSIAN 03, revision D.01, Gaussian, Inc., Wallingford, CT, 2004.
[39] MOLPRO, a package of ab initio programs, version 2006.1, H.-J. Werner, P. J. Knowles, R. Lindh, see http://www.molpro.net.
[40] MOLDEN3.4, G. Schaftenaar, CAOS/CAMM Center, The Netherlands, 1998.